Journal of Hazardous Materials 189 (2011) 801–808

Contents lists available at ScienceDirect

Journal of Hazardous Materials

journal homepage: www.elsevier.com/locate/jhazmat

Encapsulation of nZVI particles using a Gum Arabic stabilized oil-in-water emulsion

Tao Long [a], C. Andrew Ramsburg [b,*]

[a] Nanjing Institute of Environmental Sciences, Chinese Ministry of Environmental Protection, No. 8 Jiangwangmiao Street, Nanjing 210042, Jiangsu, China
[b] Department of Civil and Environmental Engineering, Tufts University, 200 College Avenue, Room 113 Anderson Hall, Medford, MA 02155, USA

ARTICLE INFO

Article history:
Received 22 October 2010
Received in revised form 10 February 2011
Accepted 28 February 2011
Available online 5 March 2011

Keywords:
Zero valent iron
Nanoparticles
Emulsion
Encapsulation
Source zone

ABSTRACT

Stabilization of reactive iron particles against aggregation and sedimentation is a critical engineering aspect for successful application of nZVI (nanoscale zero valent iron) within the contaminated subsurface environment. In this work we explore the stability and reactivity of a new encapsulation approach that relies upon Gum Arabic to stabilize high quantities of nZVI (~12 g/L) in the dispersed phase of a soybean oil-in-water emulsion. The emulsion is kinetically stable due to substantial repulsive barriers to droplet–droplet induced deformation and subsequent coalescence. Sedimentation time scales were found to be on the order of hours ($\tau = 4.77 \pm 0.02$ h). Thus, the use of Gum Arabic represents an advance in stabilizing nZVI-in-oil-in-water emulsions. nZVI within the emulsion was shown to be reactive with both TCE degradation and H_2 production observed. Degradation rates were observed to be on the same order of magnitude as those reported for less stable, aqueous suspensions of nZVI. TCE consumption within the emulsion was described with an equivalent aqueous phase rate coefficient of $\sim 5 \times 10^{-4} L_{aq}/m^2$ h.

1. Introduction

When suspended within an aqueous phase, nZVI (nanoscale zero valent iron) particles tend to rapidly agglomerate due to the dominance of attractive forces such as magnetic forces [1]. Aggregation increases particle settling and leads to greater particle retention. Thus, the principal limitation to application of nZVI within the subsurface remediation is particle mobility. To overcome this limitation several classes of stabilization mechanisms have been developed including: grafting of high molecular materials to the surface of nZVI particles [2–6]; coating Fe^0 on the surface of non-magnetic carrier materials [7–9]; enhancing solution viscosity to limit aggregation and settling [10,11]; and encapsulation of nZVI within transport vessels [12,13].

Our previous studies highlight the benefits of encapsulating nZVI within the oil droplets of an oil-in-water emulsion when considering iron-based treatment of DNAPL source zones [13,14]. Key among these benefits is the ability to transport well-designed oil-in-water emulsions through porous media with modest energy input [14–16]. In fact, delivery of g/L quantities of nZVI at Darcy velocities which are readily maintained in shallow, unconfined aquifers containing DNAPL source zones (i.e., <1 m/d) is an important advantage offered by encapsulation approaches; since injections of aqueous suspensions of nZVI typically rely upon Darcy velocities on the order of 10–100 m/d to transport the nZVI [13]. Encapsulating iron particles within a nonpolar phase can also limit the oxidation of Fe^0 by water (and non-target solutes). These side reactions can cause significant loss of nZVI effectiveness, particularly in aqueous-based delivery approaches [17]. Encapsulation strategies, however, must be carefully designed to control reactivity. Recently, Berge and Ramsburg [13,18] have demonstrated the capability of nZVI to degrade chlorinated solvents within organic phases when water is available as a solute within the organic phase. The stability of the nZVI containing (2.5 g/L) oil-in-water emulsion created by Berge and Ramsburg [13] was based upon, however, required coating the nZVI prior to incorporation within the non-polar phase and the use of two surfactants to stabilize (energetically) the oil–water interface. Kinetic stability of these emulsions was limited because the magnetic, nZVI containing oil droplets are difficult to stabilize using energetic approaches (i.e., surfactants to lower the interfacial energy) [13]. The combination of modest stability and the fact that surface coatings have been found to reduce the reactivity of nZVI by about an order or magnitude [3] suggest the need for a new encapsulation approach. This manuscript explores the utility of using Gum Arabic to stabilize a soybean oil-in-water emulsion containing a high concentration (~10 g/L) of uncoated nZVI particles. Gum Arabic (GA) was selected because it is natural, non-toxic material produced from the tree sap of *Acacia* senegal, *Acacia* seyal or *Acacia* polyacantha that is

* Corresponding author. Tel.: +1 617 627 4286; fax: +1 617 627 3994.
E-mail addresses: longtao@nies.org (T. Long), andrew.ramsburg@tufts.edu (C.A. Ramsburg).

0304-3894/$ – see front matter © 2011 Elsevier B.V. All rights reserved.
doi:10.1016/j.jhazmat.2011.02.084

frequently employed in the food industry for structural stabilization and encapsulation (i.e., wrapping of the interface), as well as control of texture, color and flavor [19–22]. Our experimental and theoretical assessment of stability is completed within the context of maintaining reactivity (with a model contaminant, trichloroethene) at rates comparable to those observed for aqueous suspensions of nZVI.

2. Materials and methods

2.1. Materials

Ferrous sulfate ($FeSO_4{\cdot}7H_2O$), hydrochloric acid (HCl)·(37%), sodium hydroxide (NaOH), methanol (99.9%), oleic acid and trichloroethylene (TCE) (99.9%) were supplied by Fischer Scientific. Sodium borohydride (NaBH4) (98+%) and Gum Arabic were supplied by Acros Organics. Soybean oil was purchased from MP Biochemicals. Purified water (resistivity >18.2 MΩ cm and total organic carbon (TOC) <10 ppb) was obtained from a MilliQ Gradient A-10 station (Millipore Inc.). nZVI was synthesized by reducing ferrous ion with sodium borohydride using a method modified from that of Liu et al. [23] to produce 30–40 nm size particles [18]. The details of the synthesis are available in Supporting data. N_2 BET surface area of the nZVI (8 m^2/g) was conducted by Particle Technology Labs (Downers Grove, IL) using a Micromeritics TriStar 3000 static pressure surface area analyzer.

2.2. Emulsion characterization

The nZVI-in-oil-in-water emulsion created in this study was a dark-grey, opaque fluid (Fig. 1a) comprising GA (10.0 wt%), soybean oil (9.0 wt%), oleic acid (2.2 wt%), iron (1.2 wt%), methanol (0.4 wt%) and water (77.2 wt%). The Fe^0 content of the emulsion (12 g/L), confirmed by acid digestion, is greater than the iron content often considered for application within the subsurface (1–10 g/L) [13,24]. Information related to the formulation and construction of the emulsion may be found in Supporting data. The ZVI content of the emulsion was quantified using an acid digestion procedure [13]. Methods employed to determine the density, viscosity, interfacial tension with TCE-NAPL, as well as methods to visualize the emulsion using light microscopy were similar to those previously reported [13]. Details are provided in Supporting data. The stability of the emulsion was assessed using multiple methods: visual assessment of the time to first destabilization; dynamic light scattering, and sedimentation studies. It should be recognized that robust emulsion characterization relies upon multiple lines of evidence since techniques that involve plating or dilution may alter the emulsion [13]. Stability of the emulsion at 100× dilution was assessed via light transmittance at 580 nm over a period of 24 h using a Lambda 25 spectrophotomer (PerkinElmer, Inc.). Droplet size distributions at 1000× dilution were quantified via dynamic light scattering (DLS) using a Zetasizer NanoZS analyzer (Malvern). Dynamic light scattering measurements were accomplished at 633 nm, 173°. Droplet size distributions are produced from the intensity measurements using an exponentially decaying, standard autocorrelation coefficient that is related to the hydrodynamic diameter through the Stokes–Einstein equation. Zeta potential was measured with laser Doppler velocimetry (LDV) at 1000× dilution using the same Zetasizer Nano-ZS analyzer.

2.3. Emulsion reactivity

nZVI containing emulsion (~40 g) was added to a series of 120 mL glass serum bottles inside an argon filled glove box. All batch experiments were performed in triplicate with iron controls constructed using the blank emulsion (see Supporting data). Subsequent to the addition of ~15 mmol of TCE (save TCE control systems) reactors were sealed and rotated on LabQuake™ end-to-end shakers at 8 RPM. The molar ratio of TCE to Fe^0 for these experiments was 1.8 mol/mol (i.e., reactions were iron limited). Headspace gas in the reactors were sampled successively, and analyzed for hydrogen and TCE using GC-TCD and GC-FID, respectively. Details of the GC methods are available in Supporting data. Phases were assumed to be in equilibrium given the large surface area represented by the emulsion droplets, and the rapid partitioning reported for completely mixed reactors [25]. The relevant partition coefficients for TCE and H_2 are $351L_{aq}/L_{oil}$ [26] and $0.08L_{aq}/L_{oil}$ [18], respectively. Henry's coefficients for TCE and H_2 are $0.083L_{aq}/L_{gas}$ [25] and $51.1L_{aq}/L_{gas}$, respectively [27].

3. Results and discussion

3.1. Emulsion stability

3.1.1. Visual assessment of emulsion stability

Visual inspection suggested the GA stabilized emulsion has kinetic stability in excess of 4 h (i.e., no discernible phase separation was observed during this time frame). Destabilization over longer time (4 days) was found to occur via sedimentation (dispersed phase (iron oil + GA) density was 1.15 g/mL) with ~20% volume observed at the bottom of the tube containing the emulsion. Sedimented emulsion droplets were readily resuspended by inverting the tube suggesting limited coalescence (emulsions broken through coalescence generally require much greater energy input to reform the large surface area represented by suspended droplets) [28]. Light microscopy examination of diluted suspended phase suggests droplet sizes of ~1 μm and smaller (Fig. 1b) which compares favorably to the number average droplet diameter (1.03 μm) obtained from DLS (Fig. 2). In addition, aggregates of nZVI particles were not observed in any image suggesting the iron remained encapsulated within the dispersed phase.

Oil-in-water emulsions in which the dispersed phase density that is greater than the continuous phase density generally destabilize via sedimentation, coalescence, and/or Ostwald ripening. Ostwald ripening is not relevant for emulsion studied here given the low aqueous solubility of the soybean oil constituents (primarily linoleic and oleic acids, see Supporting data). The potential roles of sedimentation and coalescence were considered here through a series of experiments that began with light microscopy imaging of the *settled* emulsion (Fig. 1c). Shown in Fig. 1c are larger opaque droplets found among chains of smaller opaque droplets. The observation of aggregated droplets, particularly those having diameters of several microns, is indicative of an attractive magnetic body force between ferromagnetic dipoles. These observations, coupled with the absence of nZVI aggregates in either the emulsion or settled emulsion suggest: (i) that the GA wrapping provides a competent barrier to coalescence (this observation is further explored in Section 3.1.2); and (ii) the droplets contain the iron. The lack of coalescence and the observation that the droplets are readily resuspended suggest that the emulsion is destabilized by aggregation of the iron-containing oil droplets, with sedimentation occurring over a long time scales (this assessment if further explored in Section 3.1.3).

3.1.2. Droplet coalescence

To explore the potential role of coalescence, a time course of droplet size distributions were obtained via DLS with sampling occurring after gently inverting the tube 3–4 times to eliminate the potential influence of sedimentation. Results of the time series are shown in Fig. 2, where the similarity between the droplet size distributions through the observation period suggest that coales-

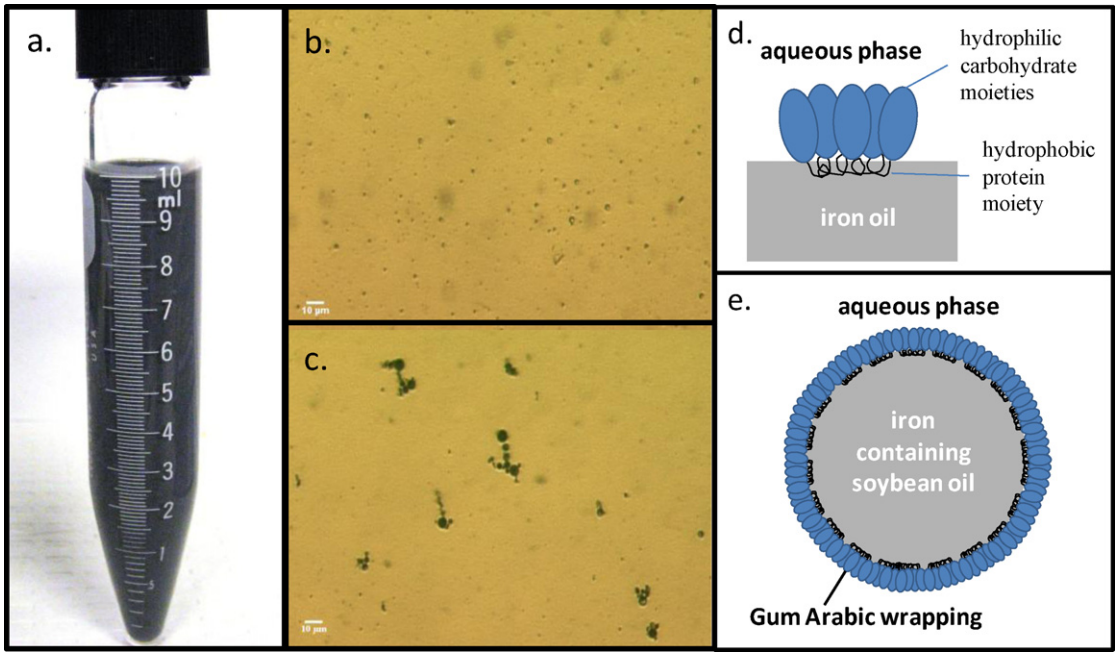

Fig. 1. GA stabilized, iron containing, oil-in-water emulsion: (a) photograph; light microscopy images of the suspended (b) and sedimented (c) fractions (with 10 μm scale bar); conceptual diagram of (d) adsorption of GA to iron oil (after Ref. [19]), and (e) stabilized droplet.

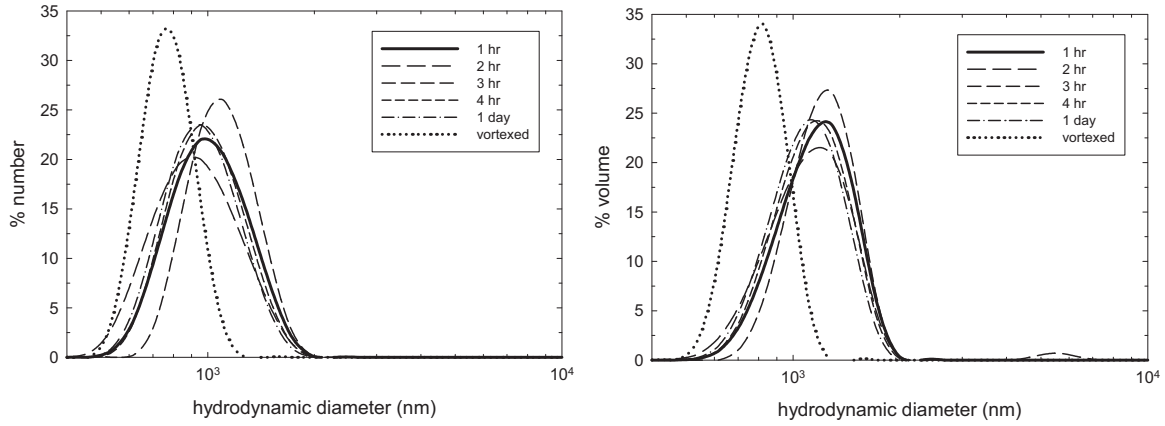

Fig. 2. Droplet size distributions over the period of 1 day plotted on the basis of number (left) and volume (right).

cence plays little role in destabilizing this emulsion. Coalescence (i.e., the rupture of droplet membranes to form one, larger droplet) would result in a substantial increase in the frequency of the largest droplets. This is not evident even in the droplet size distributions plotted on a percent volume basis (which accentuates the presence of large droplets). To further explore the potential role of coalescence, the emulsion was vortexed (Fisher Vortex Genie 2) for 1 min following the 24 h sample to produce a number average droplet diameter of 0.78 μm. The input of the large quantity of energy provided by the vortexer resulted in a small change in the droplet size distribution suggesting there are few coalesced droplets to be broken and resuspended after 1 day.

The observed stability against coalescence in the presence of the magnetic attraction between the nZVI containing oil droplets is thought to result from the structural stability provided by the GA film. GA has a complex molecular structure comprising a hydrophobic protein rich backbone to which many hydrophilic carbohydrate blocks are attached [19]. At the water–oil interface, the protein groups strongly associate with the oil phase, leaving the carbohydrate blocks protruding outwards in the aqueous phase which form a physical macromolecular film around the oil droplets. Once formed, the viscoelasticity of the film can be maintained even when the emulsion is diluted, particularly when the GA to oil mass ratio is approximately 1:1 [19].

3.1.3. Droplet aggregation and sedimentation

Droplet sedimentation was quantitatively examined using light transmission over a 24 h period, with a quasi-steady state found around 16 h (Figure SD-1). Recall that visual assessment of emulsion stability suggests destabilization occurs over the period of days. Thus it appears there is a fraction of the emulsion which slowly settles (i.e., between 16 h and 4 days). Nicolosi et al. [29] modeled similar behavior by conceptualizing the suspension as comprising settling and non-settling fractions to obtain time constants for the sedimentation process. Following their approach (summarized in Supporting data), we identified two sedimenting populations and one non-sedimenting population. In contrast to studies employing linearization schemes to determine the time constants associated with particle/droplet settling, we fit (Equation SD-E1) Equation SD-E1 to the data set using a non-

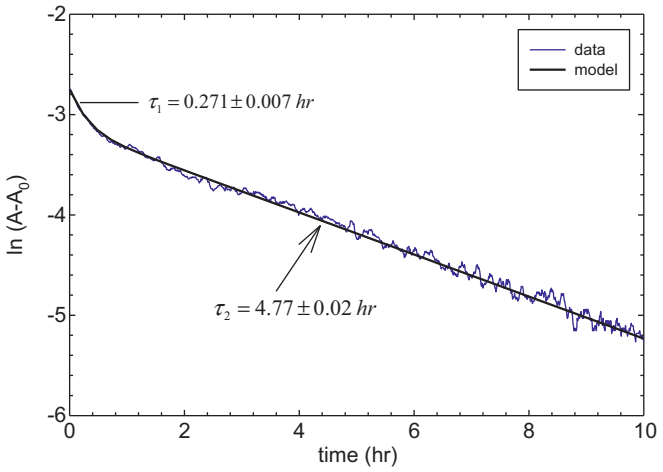

Fig. 3. Sedimentation data and model fit with time constants for the two settling populations shown. See supporting data for details on sedimentation model.

linear least squares approach (Figure SD-1). Time scales for the sedimenting fractions were found to be $\tau_1 = 0.271 \pm 0.007$ h and $\tau_2 = 4.77 \pm 0.02$ h which are shown in Fig. 3 in a manner that better visualizes the two settling populations. The short time scale process likely results from sedimentation of the large droplets shown to be present in both the light microscopy and DLS analyses. Consideration of the longer time scale process begins to make apparent one benefit of emulsion encapsulation – slower gravitational destabilization. This benefit coupled with the observation that gentle mixing re-stabilizes the emulsion suggests that GA emulsion may stabilize the nZVI over time-scales consistent with transport through porous media [13,30].

The time scale for sedimentation quantified here is a phenomenological description of a complex settling process. To better understand the role of aggregation in the gravitational destabilization of the emulsion, we consider a highly simplified Stokes law analysis for purposes of illustration. An isolated, rigid droplet that is 1 μm in size ($\rho = 1.15$ g/mL) settling through an otherwise quiescent aqueous phase ($\rho = 1.00$ g/mL and $\mu = 1.00$ mPa s) attains steady-state velocity of ~7 mm/d. Considering this slow, albeit ideal, sedimentation velocity with the observation of aggregates in the sedimented fraction of the light microscopy analysis (Fig. 1c), we hypothesize that the destabilization observed over the first 16 h of the study resulted from droplet aggregation which hastened sedimentation. In addition, we hypothesize that the non-sedimenting fraction of the emulsion represents a size fraction that is kinetically stable against the coupled aggregation–sedimentation process.

3.1.4. Droplet–droplet interactions

To explore the hypotheses related to aggregation and sedimentation illustrative, like–like interactions between 600 nm and 1100 nm droplets were qualitatively assessed using extended DLVO theory for deformable emulsion droplets [31–33]. Details of the DLVO analysis including equations and all parameter values are provided in Supporting data. In short, the analysis included van der Waals (VW) and magnetic (M) attractive interactions with electrostatic (ES), steric (St), interfacial dilatation (S), interfacial bending (B), and hydration (H) repulsive interactions. It is noted that of these interactions, hydration, interfacial dilatation and interfacial bending are all short range forces that become important when assessing the potential for droplet deformation. The shape of aggregated droplets is important because deformed droplets represent strong aggregation on an energetic path toward coalescence (i.e., film rupture) [33]. Droplet deformation, as assessed by the dimension associated with the flattening of the interface (r, see Figure SD-2), occurs when attractive forces (van der Waals and magnetic) are stronger than long range repulsive forces (electrostatic and steric) and those forces resulting from increased interfacial area (hydration, interfacial dilatation, and interfacial bending).

Illustrative results from the DLVO analysis are shown in Fig. 4 with deformation (r) and separation (s) normalized by the radius of the iron–oil core (a) (see Fig. 1d–e for conceptual model of the droplets). Calculations suggest that the minimum energy condition lies at zero deformation for both droplet sizes. This can be seen in the contour plot of deformation versus separation by the energy valley ($s = 450$ and 181 nm for the 600 and 1100 nm diameter droplets, respectively) that extends to the zero deformation condition ($r = 0$) [33]. It is important to note when comparing these separation distances to those dimensionless distances reported in Fig. 4 that the core radius (a) represents the nZVI-containing oil droplet without the GA wrapping (see Fig. 1d–e). The absence of deformation in these calculations is consistent with the lack of coalescence seen in the DLS measurements and suggests that the GA structure provides a competent physical–chemical barrier against the strong magnetic attraction. The barrier to droplet contact creates a near infinite stability parameter (see Equation SD-E1 for equation and description), which indicates that the energetic barrier is large enough to effectively prevent irreversible aggregation in the primary minimum [34]. Reversible aggregation, however, may still occur in the secondary minimum. In the case of the 600 nm diameter droplet, the secondary minimum (approx. −40 kT) occurs at long range (431 nm). The large separation distance and zero deformation suggest that aggregates of 600 nm droplets are relatively weak and perhaps overcome by mixing which is consistent with our observation of slow sedimentation [28,33]. In contrast, the secondary minimum associated with 1100 nm droplets represents a strong attractive force (approx.−1340 kT) that may lead to more rapid aggregation and settling – an assessment that is supported the observation of chains and clusters of relatively large droplets in the sedimented fraction (Fig. 1c). It is interesting that the droplet size distributions (Fig. 2) do not appear to be consistent the extent of aggregation expected from the strong, albeit theoretical, interaction calculated using extended DLVO theory. Thus, it is important to recall that the temporal study of droplet size distribution was conducted in the context of coalescence where the vials were inverted 3–4 times before sampling. We hypothesize that this inversion process was sufficient to separate the flocculated droplets – a hypothesis that is supported by observations that we are able to resuspend the settled emulsion (described above).

3.2. Reactivity screening

A series of batch experiments was designed to quantify apparent rate coefficients for the four-phase system (headspace, dispersed phase (oil droplets), continuous phase (aqueous phase) and nZVI) assuming the reaction occurs within the dispersed (oil) phase. Reactors were iron limited with a TCE to Fe^0 molar ratio of 1.8 mol/mol. Headspace data for both TCE and H_2 shown in Fig. 5 (averages of triplicate reactors) demonstrate reactivity in comparison with the control reactors in which the emulsion did not contain iron. Recall that phases were assumed to be in equilibrium given the large surface area represented by the emulsion droplets, and the rapid partitioning reported for completely mixed reactors [25]. Thus the control (emulsion without iron) represents the equilibrium distribution of TCE between the three fluid phases. The data suggest that over the ~300 h monitoring period, 4 mmol TCE was consumed in presence of between 17 and 24 mmol e^- (range established by assuming Fe^0 goes to Fe (II) and Fe (III), respectively).

Rate coefficients shown in Table 1 were obtained from simultaneous, weighted (inverse of standard error from triplicate reactors) fit to the reaction data. Details of the model employed to obtain the

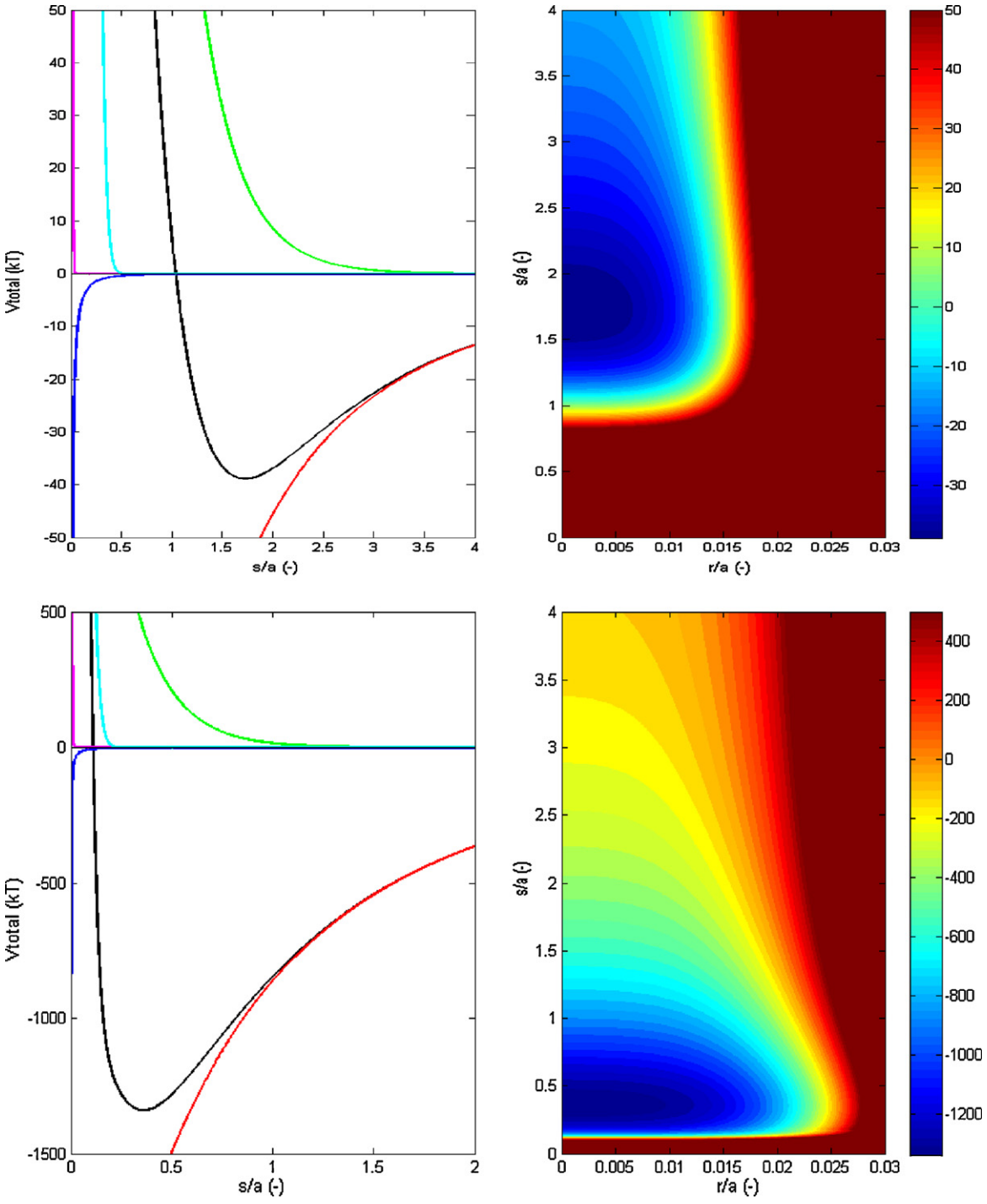

Fig. 4. Interaction energies for 600 nm (top) and 1100 nm (bottom) diameter GA wrapped droplets for zero deformation (left) and as a function of deformation (right). Plots are in terms of dimensionless separation (s/a) and dimensionless deformation (r/a), where a is the radius of the magnetic, iron oil core (i.e., 600 nm diameter GA wrapped drop has a 250 nm core radius (a) and GA wrapping thickness of 50 nm). Lines in zero deformation interactions are color coded: total (black), magnetic (red), van der Waals (blue), electrostatic (green), steric (cyan) and hydration (pink). Interfacial dilatation and surface bending are only operable for $r > 0$. Color contours correspond to interaction energies for droplets undergoing deformation. Values greater than 50 (top) and 500 kT (bottom) are shown as dark red to highlight the minimum energy state. See Figure SD-2 for schematic definition of droplet deformation. (For interpretation of the references to color in this figure legend, the reader is referred to the web version of the article.)

fitted parameters are provided in Supporting data. In brief, data were modeled by coupling reactions for pseudo first-order consumption of TCE, and pseudo-zero order production of hydrogen (given that the water content in the oil remains constant under the assumption of equilibrium partitioning). In addition, a pseudo-second order, hydrogenation reaction was included based upon the observation that boron may catalyze a reaction between H_2 and TCE [23]. Modeling results suggest approximately half of the 160 μmol H_2 produced were subsequently consumed in the hydrogenation reaction. Total ethane production, estimated using K_{ow} values for the soybean–oil partition coefficient [35] to be 25 μmol, is consistent with this amount of hydrogenation. Surprisingly little production of ethane occurred beyond what is predicted by the hydrogenation reaction (Fig. 5) suggesting coupling pathways may be enhanced within the soybean oil. Liu et al. [23] found that coupling products (C3–C6) accounted for up to 30% of the

Table 1
Fitted rate coefficients for reaction within the dispersed phase of the GA emulsion.

	Fitted rate coefficient for reaction in droplet[a] (k)	Surface normalized rate coefficient for reaction in droplet[b] (k_{SA})
TCE consumption (iron)	$(7.9 \pm 0.6) \times 10^{-3}$ (1/h)	$(1.5 \pm 0.3) \times 10^{-5}$ (L_{oil}/m^2 h)
TCE consumption (catalytic)	$(1.1 \pm 0.2) \times 10^{2}$ (L_{oil}/mmol$_{H_2}$ h)	$(2.0 \pm 0.3) \times 10^{-1}$ (L^2_{oil}/mmol$_{H_2}$ m^2 h)
H_2 production	$(4.7 \pm 0.4) \times 10^{-2}$ (mmol$_{H_2}$/L_{oil}h)	$(8.9 \pm 0.8) \times 10^{-5}$ (mmol$_{H_2}$/m^{2}h)
TCE deactivation	$(2.9 \pm 0.2) \times 10^{-2}$ 1/h	–

[a] Represents reaction rate coefficient in absence of headspace.
[b] Specific surface area of the iron particles was determined to be 8 m^2/g.

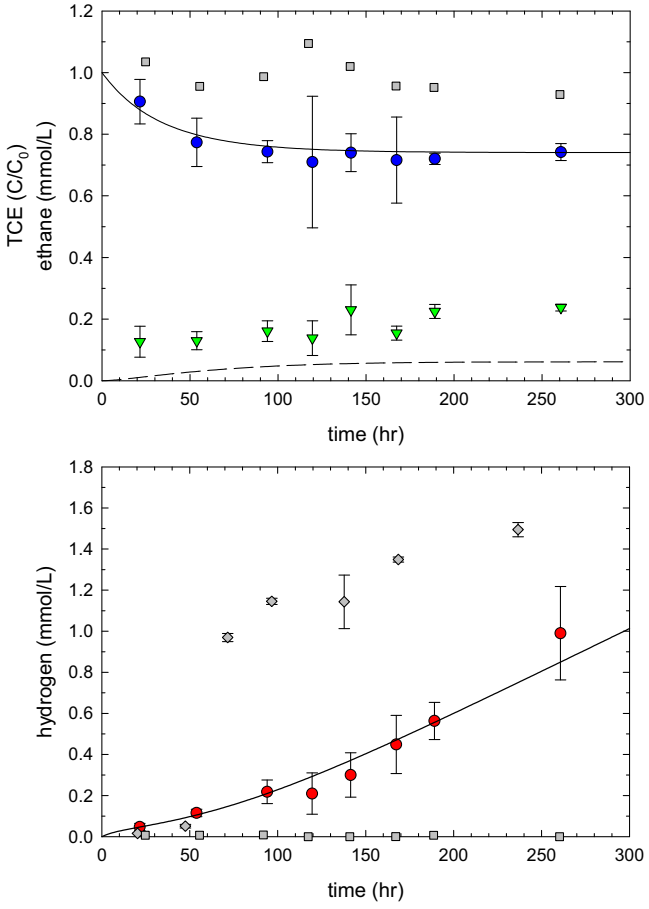

Fig. 5. Reaction data and kinetic model fit for TCE transformation by the GA stabilized emulsion. Error bars represent standard error of triplicate reactors. Headspace data and model fits for TCE (●, top) and hydrogen (●, bottom). Control reactors included absence of iron (□, top and bottom) and absence of TCE (◇, bottom). TCE and hydrogen data were simultaneous fit (solid lines) as described in Supporting data. Ethane data (▽, top) are shown with predicted concentration (dashed line) from hydrogenation reaction fit to TCE and hydrogen data.

TCE mass degraded in aqueous phase systems. We hypothesize that lack of products observed here resulted from formation of a broad distribution of coupling products that remained below our quantification limits due to partitioning (reactors contained three fluid phases). Computational and experimental studies that report a 0.5 log unit increase in K_{ow} for each carbon addition demonstrate the affinity of coupling products for the oil and support this hypothesis [35,36]. It is interesting that water remains reactive within the emulsion (as evidenced by the production of H_2) even as the reaction with TCE slows. This suggests that: sites responsible for catalyzing the conversion of TCE may be passivated (no effect on H_2 production just decrease in H_2 consumption); reactive sites on the iron surface remain accessible to water after becoming inaccessible to TCE (water can transport through porous oxides [37]); or both.

Comparison of surface normalized rate coefficients established for the reaction occurring within the droplets to those report for aqueous suspensions of nZVI must consider the capacity that the oil droplet has for chlorinated solvents. The TCE rate coefficient within the *oil droplets* can be shown to be equivalent to an aqueous phase rate coefficient of $\sim 5 \times 10^{-3} L_{aq}$/m^2 h (Equation SD-E13–E15) which is similar to rate coefficients reported for bare nZVI [23,38,39]. The emulsion, however, is ~10% oil, suggesting that conversion within the emulsion is equivalent to an aqueous phase rate coefficient of $\sim 5 \times 10^{-4} L_{aq}$/m^2 h. Berge and Ramsburg [18] employed surface normalized, maximum observed rates of TCE consumption to compare aqueous and nonaqueous reactions mediated by various types of nZVI. Maximum observed rates of TCE consumption were employed because aqueous phase reactions are limited by the solubility of TCE in water, while reactions within the nonaqueous phase are limited by the amount of water within the organic phase. Maximum observed rates were found to typically range between 1 and 200 μmol$_{TCE}$/m^2-day for Fe^0 particles and between 50 and 500 μmol$_{TCE}$/m^2-day for bimetallic particles [18]. When the equivalent rate coefficient of the GA emulsion system is applied with the solubility of TCE in water (~8 mM, [40]), the maximum observed rate of TCE consumption is ~100 μmol/m^2-day. Thus, the rate of TCE conversion in the emulsion system compares favorably to rates observed in aqueous suspensions of iron particles [12,41] while stabilizing 12 g/L Fe^0.

4. Conclusions and implications

Use of GA to structurally stabilize the oil–water interface in the emulsion permits high quantities of nZVI (>10 g Fe^0 per L emulsion) to be encapsulated within the dispersed, oil droplets. The kinetically-stable emulsion was found to destabilize via a sedimentation process that occurred over the period of days. The temporal analysis of droplet size distributions and calculated interaction energetics suggest that the GA wrapping provided a highly competent structural barrier to coalescence. nZVI within the emulsion was shown to be reactive with both TCE degradation and H_2 production observed. TCE consumption was described with an equivalent aqueous phase rate coefficient of $\sim 5 \times 10^{-4} L_{aq}$/m^2 h.

Overall the GA emulsion represents an advance in stabilizing high quantities of nZVI particles for transport in porous media while maintaining particle reactivity at rates that are consistent with polymer coated particles. Droplet sizes on the order of a micron have been shown to be mobile within fine sand due to limited potential for straining [13–16]. Moreover the net negative charge on the emulsion droplets and the ability for gentle mixing to maintain the kinetic stability suggest that the GA emulsion may be transported within porous media. The combination of the relatively high interfacial tension with TCE-NAPL (30.75 ± 0.02 mN/m) and

modest viscosity (16.8 ± 0.1 mPa s at $10\ s^{-1}$ and $20.00 \pm 0.01\ ^{\circ}C$, see Figure SD-3) suggest that the GA emulsion offers limited potential for mobilizing DNAPL during delivery (Figure SD-4 and related discussion).

The materials employed to create the emulsion (GA, soybean oil, oleic acid) are food-grade, commodity chemicals and may enhance the synergy between nZVI-based reductive dechlorination and metabolic reductive dechlorination; particularly since encapsulation of iron sequesters the chemical and biological reactions [16,24,42,43]. Immersion of the nZVI within oil immediately following particle synthesis protects the Fe^0 from oxidation by atmospheric oxygen and reaction with water, suggesting the possibility of limited decline in ZVI content during longer-term storage. Because the reaction occurs in a non-aqueous phase (oil or NAPL), the availability of dissolved water becomes critical and represents a tradeoff between TCE consumption and H_2 production [18]. While mechanistic study of the oil-based reactions was beyond the scope of the present study, the results presented here warrant follow on study to elucidate reaction pathways, as well as the influence of iron mineralogy on the reaction.

Acknowledgements

The authors gratefully acknowledge Dr. Yonggang Wang (Tufts) for his assistance with the DLS and zeta potential measurements. Drs. Nicole Berge (University of South Carolina) and David Wilbur (Tufts) are acknowledged for their helpful discussions related the experimental protocols and analytical methods employed herein. In addition we wish to acknowledge the constructive comments provide by four anonymous reviewers. This research was supported by the U.S. Department of Defense, through the Strategic Environmental Research & Development Program under Project ER-1487. The content of this paper does not necessarily represent the views of the sponsor.

Appendix A. Supplementary data

Supplementary data associated with this article can be found, in the online version, at doi:10.1016/j.jhazmat.2011.02.084.

Supplementary data includes: nZVI synthesis and analytical methods; emulsion formulation and characterization; extended DLVO equations and parameters; kinetic modeling of reactivity and associated parameters; emulsion viscosity; and, considerations for application of emulsions in DNAPL source zones.

References

[1] T. Phenrat, N. Saleh, K. Sirk, R.D. Tilton, G.V. Lowry, Aggregation and sedimentation of aqueous nanoscale zerovalent iron dispersions, Environ. Sci. Technol. 41 (2007) 284–290.
[2] F. He, D.Y. Zhao, Manipulating the size and dispersibility of zerovalent iron nanoparticles by use of carboxymethyl cellulose stabilizers, Environ. Sci. Technol. 41 (2007) 6216–6221.
[3] T. Phenrat, N. Saleh, K. Sirk, H.J. Kim, R.D. Tilton, G.V. Lowry, Stabilization of aqueous nanoscale zerovalent iron dispersions by anionic polyelectrolytes: adsorbed anionic polyelectrolyte layer properties and their effect on aggregation and sedimentation, J. Nanopart. Res. 10 (2008) 795–814.
[4] Y.P. Sun, X.Q. Li, W.X. Zhang, H.P. Wang, A method for the preparation of stable dispersion of zero-valent iron nanoparticles, Colloids Surf. A 308 (2007) 60–66.
[5] A. Tiraferri, K.L. Chen, R. Sethi, M. Elimelech, Reduced aggregation and sedimentation of zero-valent iron nanoparticles in the presence of guar gum, J. Colloid Interface Sci. 324 (2008) 71–79.
[6] W. Wang, M. Zhou, Z. Jin, T. Li, Reactivity characteristics of poly(methyl methacrylate) coated nanoscale iron particles for trichloroethylene remediation, J. Hazard. Mater. 173 (2010) 724–730.
[7] B. Schrick, B.W. Hydutsky, J.L. Blough, T.E. Mallouk, Delivery vehicles for zerovalent metal nanoparticles in soil and groundwater, Chem. Mater. 16 (2004) 2187–2193.
[8] T.H. Zheng, J.J. Zhan, J.B. He, C. Day, Y.F. Lu, G.L. McPherson, G. Piringer, V.T. John, Reactivity characteristics of nanoscale zerovalent iron-silica composites for trichloroethylene remediation, Environ. Sci. Technol. 42 (2008) 4494–4499.
[9] J.J. Zhan, B. Sunkara, L. Le, V.T. John, J.B. He, G.L. McPherson, G. Piringer, Y.F. Lu, Multifunctional colloidal particles for in situ remediation of chlorinated hydrocarbons, Environ. Sci. Technol. 43 (2009) 8616–8621.
[10] E. Dalla Vecchia, M. Luna, R. Sethi, Transport in porous media of highly concentrated iron micro- and nanoparticles in the presence of Xanthan Gum, Environ. Sci. Technol. 43 (2009) 8942–8947.
[11] S. Comba, R. Sethi, Stabilization of highly concentrated suspension of iron nanoparticles using shear-thining gels of Xanthan Gum, Water Res. 43 (2009) 3717–3726.
[12] J. Quinn, C. Geiger, C. Clausen, K. Brooks, C. Coon, S. O'Hara, T. Krug, D. Major, W.S. Yoon, A. Gavaskar, T. Holdsworth, Field demonstration of DNAPL dehalogenation using emulsified zero-valent iron, Environ. Sci. Technol. 39 (2005) 1309–1318.
[13] N.D. Berge, C.A. Ramsburg, Oil-in-water emulsions for encapsulated delivery of reactive iron particles, Environ. Sci. Technol. 43 (2009) 5060–5066.
[14] J.J. Crocker, N.D. Berge, C.A. Ramsburg, Encapsulated delivery of reactive iron particles using oil-in-water emulsions, in: M.G. Trefry (Ed.), Groundwater Quality: Securing Groundwater Quality in Urban and Industrial Environments, IAHS Publication No. 324, Wallingford, Oxfordshire, United Kingdom, 2008, pp. 242–249.
[15] K.M. Coulibaly, R.C. Borden, Impact of edible oil injection on the permeability of aquifer sands, J. Contam. Hydrol. 71 (2004) 219–237.
[16] R.C. Borden, Effective distribution of emulsified edible oil for enhanced anaerobic bioremediation, J. Contam. Hydrol. 94 (2007) 1–12.
[17] P.G. Tratnyek, R.L. Johnson, Nanotechnologies for environmental cleanup, Nano Today 1 (2006) 44–48.
[18] N.D. Berge, C.A. Ramsburg, Iron-mediated trichloroethene reduction within non-aqueous phase liquid, J. Contam. Hydrol. 118 (2010) 105–116.
[19] E. Dickinson, Hydrocolloids at interfaces and the influence on the properties of dispersed systems, Food Hydrocolloids 17 (2003) 25–39.
[20] A.M. Islam, G.O. Phillips, A. Sljivo, M.J. Snowden, P.A. Williams, A review of recent developments on the regulatory, structural and functional aspects of gum arabic, Food Hydrocolloids 11 (1997) 493–505.
[21] M.L. Jayme, D.E. Dunstan, M.L. Gee, Zeta potentials of Gum Arabic stabilised oil in water emulsions, Food Hydrocolloids 13 (1999) 459–465.
[22] S. Motlagh, P. Ravines, Q. Ma, F. Jaksch, Identification of gum Arabic using PAGE and IEF, in: P. Williams, G. Phillips (Eds.), Gums and Stabilisers for the Food Industry vol. 10, Royal Society of Chemistry, 1999, pp. 53–58.
[23] Y.Q. Liu, S.A. Majetich, R.D. Tilton, D.S. Sholl, G.V. Lowry, TCE dechlorination rates, pathways, and efficiency of nanoscale iron particles with different properties, Environ. Sci. Technol. 39 (2005) 1338–1345.
[24] T.L. Kirschling, K.B. Gregory, E.G. Minkley, G.V. Lowry, R.D. Tilton, Impact of nanoscale zero valent iron on geochemistry and microbial populations in trichloroethylene contaminated aquifer materials, Environ. Sci. Technol. 44 (2010) 3474–3480.
[25] J.M. Gossett, Measurement of Henry's law constants for C1 and C2 chlorinated hydrocarbons, Environ. Sci. Technol. 21 (1987) 202–208.
[26] P. Pfeiffer, A.R. Bielefeldt, T. Illangasekare, B. Henry, Partitioning of dissolved chlorinated ethenes into vegetable oil, Water Res. 39 (2005) 4521–4527.
[27] D.R. Lide, Handbook of Chemistry and Physics, 88th ed., CRC Press, Boca Raton, FL, 2008.
[28] P. Becher, Emulsions: Theory and Practice, 3rd ed., Oxford University Press, Washington DC., 2001.
[29] V. Nicolosi, D. Vrbanic, A. Mrzel, J. McCauley, S. O'Flaherty, C. McGuinness, G. Compagnini, D. Mihailovic, W.J. Blau, J.N. Coleman, Solubility of $Mo_6S_{4.5}I_{4.5}$ nanowires in common solvents: a sedimentation study, J. Phys. Chem. B 109 (2005) 7124–7133.
[30] C.A. Ramsburg, K.D. Pennell, T.C.G. Kibbey, K.F. Hayes, Refinement of the density-modified displacement method for efficient treatment of tetrachloroethene source zones, J. Contam. Hydrol. 74 (2004) 105–131.
[31] I.B. Ivanov, K.D. Danov, P.A. Kralchevsky, Flocculation and coalescence of micron-size emulsion droplets, Colloids Surf. A 152 (1999) 161–182.
[32] N.D. Denkov, D.N. Petsev, K.D. Danov, Flocculation of deformable emulsion droplets: I. droplet shape and line tension effects, J. Colloid Interface Sci. 176 (1995) 189–200.
[33] D.N. Petsev, N.D. Denkov, P.A. Kralchevsky, Flocculation of deformable emulsion droplets: II. interaction energy, J. Colloid Interface Sci. 176 (1995) 201–213.
[34] B.V. Derjaguin, Theory of Stability of Colloids and Thin Films, Consultants Bureau, New York, NY, 1989.
[35] J. Sangster, Octanol–Water Partition Coefficients: Fundamentals and Physical Chemistry, Wiley, New York, NY, 1997.
[36] N.M. Garrido, A.J. Queimada, M. Jorge, E.A. Macedo, I.G. Economou, 1-Octanol/water partition coefficients of n-alkanes from molecular simulations of absolute solvation free energies, J. Chem. Theory Comput. 5 (2009) 2436–2446.
[37] J. Wang, J. Farrell, Investigating the role of atomic hydrogen on chloroethene reactions with iron using TAFEL analysis and electrochemical impedance spectroscopy, Environ. Sci. Technol. 37 (2003) 3891–3896.
[38] Y. Liu, T. Phenrat, G.V. Lowry, Effect of TCE concentration and dissolved groundwater solutes on NZVI-promoted TCE dechlorination and H_2 evolution, Environ. Sci. Technol. 41 (2007) 7881–7887.
[39] H. Song, E.R. Carraway, Catalytic hydrodechlorination of chlorinated ethenes by nanoscale zero-valent iron, Appl. Catal. B 78 (2008) 53–60.

[40] C.A. Ramsburg, K.D. Pennell, Density-modified displacement for dense nonaqueous-phase liquid source-zone remediation: density conversion using a partitioning alcohol, Environ. Sci. Technol. 36 (2002) 2082–2087.
[41] T. Phenrat, Y.Q. Liu, R.D. Tilton, G.V. Lowry, Adsorbed polyelectrolyte coatings decrease Fe^0 nanoparticle reactivity with TCE in water: conceptual model and mechanisms, Environ. Sci. Technol. 43 (2009) 1507–1514.
[42] Z.M. Xiu, Z.H. Jin, T.L. Li, S. Mahendra, G.V. Lowry, P.J.J. Alvarez, Effects of nano-scale zero-valent iron particles on a mixed culture dechlorinating trichloroethylene, Bioresour. Technol. 101 (2010) 1141–1146.
[43] R.J. Barnes, O. Riba, O.M.N. Gardner, A.C. Singer, S.A. Jackman, I.P. Thompson, Inhibition of biological TCE and sulphate reduction in the presence of iron nanoparticles, Chemosphere 80 (2010) 554–562.